Structural Engineering and Mechanics, *Vol. 10, No. 6 (2000) 577-587*
DOI: http://dx.doi.org/10.12989/sem.2000.10.6.577

Nonlinear analysis on concrete-filled rectangular tubular composite columns

Xilin Lu† and Yong Yu‡

Research Institute of Engineering Structures, Tongji University, Shanghai 200092, China

Tanaka Kiyoshi‡ and Sasaki Satoshi‡

Technical Research Institute of Fujita Corporation, Japan

Abstract. A 3D nonlinear finite element computation model is presented in order to analyze the concrete filled rectangular tubular (CFRT) composite structures. The concrete material model is based on a hypo-elastic orthotropic approach while the elasto-plastic hardening model is employed for steel element. The comparisons between experimental and analytical results show that the proposed model is a relatively simple and effective one. The analytical results show that the capacity of inner concrete of CFRT column mainly depends on the two diagonal zones, and the confining effect of CFRT section is mainly concentrated on the corner zones. At the ultimate state, the side concrete along the section cracks seriously, and the corner concrete softens with the increase of compressive strains until failure.

Key words: concrete filled rectangular tubular structure; nonlinear analysis; finite element method.

1. Introduction

In recent years, concrete-filled rectangular steel tubular (CFRT) column has become popular in structural applications due to its excellent structural behavior, and more attention has been paid to the theoretical and experimental investigations on its structural behavior. However, on the aspect of load-carrying and deformation behavior, most of the research achievements are the formula based on tested results or simple analysis by use of one-dimensional or two-dimensional finite element model. Because of the high complexity of the problem, no efficient analytical method is reported to study the load-carrying and failure mechanism of CFRT structures so far. All these considerations highlight the necessity of developing fully three-dimensional computational model which may be used to analyze CFRT composite structures. There are two aims of this paper. One is to develop a 3D finite element model for nonlinear analysis of plain concrete up to failure, and the other is to use this model to investigate the structural behavior of CFRT columns.

† Professor
‡ Research Engineer

2. Concrete material model

In finite element analysis, it is necessary to keep the model as simple as possible so that it can be easily implemented in structural analysis. And the model must be capable of idealizing the nonlinear behavior of concrete structures and can trace the overall behavior of these structures up to ultimate load, within an engineering degree of accuracy. Thus the model implemented in this paper employs three basic features to describe the material behavior, namely, (i) a nonlinear stress-strain relation including strain-softening; (ii) failure envelopes that define cracking in tension and crushing in compression, and (iii) a strategy to model the post-cracking and crushing behavior of the material. In the solution, the material can be subjected to cyclic loading conditions, i.e., the numerical solution allows for unloading and reloading including deactivation of tensile failures. However, as will become apparent, the cyclic loading conditions are only modeled realistically in essentially proportional loading.

Perfect bond is maintained between the steel element and concrete element in this paper, as has been typical in most analytical studies of concrete-filled tube members to date (e.g., Neogi 1969, Tomii 1979, Shair-Khalil and Zeghiche 1989). Also local buckling is not simulated in this model because many tests have been shown that local buckling of steel plate in CFRT columns has been prevented by infilled concrete in most cases.

2.1. Behavior in compression

The hypoelastic orthotropic model proposed by Yu and Lu (1998) is used to describe the constitutive relation of concrete under multiaxial compressive stress state. The failure criterion by Ottosen and nonlinear expression by Sargin were adopted in the model and the equivalent uniaxial strain concept was incorporated and extended to the nonlinear three-dimensional incremental stress-strain relationship. The predictions of the model were compared with some of the two-dimensional tests of Kupfer, *et al*. and some of the three-dimensional tests of Kotsovos *et al*., which showed that the model is a relatively simple and effective one with a good accuracy.

The incremental stress-strain relationship matrix is as follows:

$$[\boldsymbol{D}]=\frac{1}{\psi}\begin{bmatrix} E_1(1-\mu_{23}^2) & \sqrt{E_1E_2}(\mu_{13}\mu_{23}+\mu_{12}) & \sqrt{E_1E_3}(\mu_{12}\mu_{23}+\mu_{13}) & 0 & 0 & 0 \\ & E_2(1-\mu_{13}^2) & \sqrt{E_2E_3}(\mu_{12}\mu_{13}+\mu_{23}) & 0 & 0 & 0 \\ & & E_3(1-\mu_{12}^2) & 0 & 0 & 0 \\ & & & G_{12}\psi & & \\ & \text{symmetric} & & & G_{23}\psi & \\ & & & & & G_{13}\psi \end{bmatrix} \quad (1)$$

When taking the uniaxial condition into consideration, the concrete constitutive model is shown in Fig. 1.

2.2. Behavior in tension

In the present work, concrete in tension is modeled as a linear elastic-strain softening material and

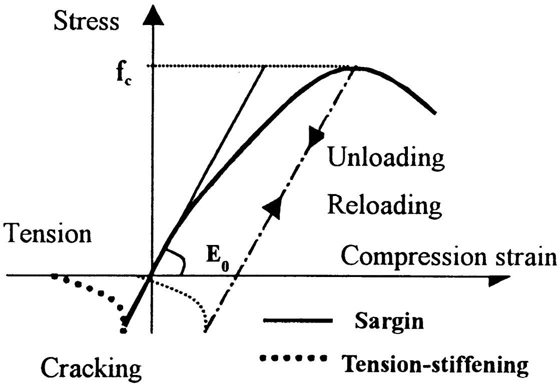

Fig. 1 Concrete model for uniaxial stress-strain

the maximum tensile stress criteria is employed to distinguish elastic behavior from tensile fracture. The limiting value defining the onset of cracking is established as follows:

(i) in the triaxial tension zone

$$f_{ti}'=f_t; \qquad (i=1,\ 2,\ 3) \tag{2}$$

(ii) for tension-tension-compression and tension-compression-compression stress states

$$f_t'=f_t(1-\sigma_{p3}/f_c); \qquad \sigma_{p3}<0 \tag{3}$$

$$f_t'=f_t(1-\sigma_{p2}/f_c)\cdot(1-\sigma_{p3}/f_c); \qquad \sigma_{p2},\sigma_{p3}<0 \tag{4}$$

Where f_t is the tensile strength of concrete. The resulting cracking surfaces are shown in Fig. 2.

The smeared crack model is used herein. For a previously uncracked sampling point, the principal stresses and their directions are evaluated. If the maximum principal stress exceeds a limiting value, a crack is formed in a plane orthogonal to this stress. Thereafter, the behavior of the concrete is no longer isotropic, and the local material axes coincide with the principal stress directions. It should be noted that the direction of the crack remains fixed thereafter, which is known as the fixed crack approach. Two sets of cracks are allowed to form at each sampling point. For simplicity, the crack directions are assumed to be orthogonal. Once the first set cracks are formed at a point, a search is

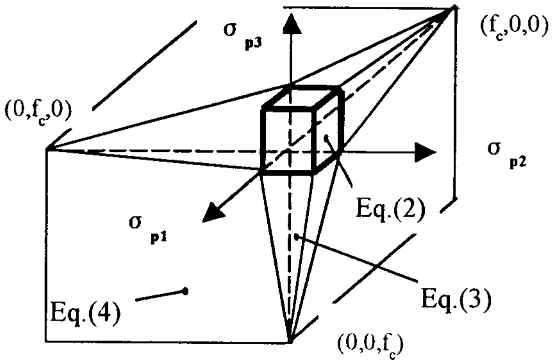

Fig. 2 Triaxial tensile failure envelop

performed in the orthogonal plane to determine the maximum stress in that plane and its direction. Again, if that stress exceeds a limiting value, a new set of cracks are assumed to form and the local material axes are fixed.

2.3. Strain-softening rule

Because the classical "tension stiffening" effect, which was explained in terms of bond interaction with reinforcing steel, cannot be applied to plain concrete structures or concrete-filled steel tube structures whose inner concrete locates at a certain distance from the interface, the approach proposed by Petersson (Bangash 1989) is used herein. The tension-stiffening curve adopted in this paper is shown in Fig. 3. The stress normal to the crack does not drop to zero immediately when the crack is formed. It decreases with increasing crack width, $\boldsymbol{w}$, or with the nominal "tensile strain $\boldsymbol{w/l_c}$". Many curves have been suggested, with linear, multi-linear, parabolic, exponential forms, etc. The manner in which parameters defining the tension-stiffening curve are chosen is more critical than its actual shape. The model proposed by Petersson (Bangash 1989) in the context of fracture mechanics is used herein, which assumes fracture energy, $\boldsymbol{G_f}$, to be a material property. The implementation of the "$\boldsymbol{G_f}$ = const." concept leads to two important conclusions: (1) the local strain-softening law depends on a characteristic length, $\boldsymbol{l_c}$; and (2) the local constitutive relation depends on the finite element mesh. An exponential curve is used to simulate the tension-stiffening effect, then

$$\sigma=\boldsymbol{f_t}(\exp(-(\varepsilon-\varepsilon_0)/\alpha)) \tag{5}$$

in which ε is nominal tensile strain in the cracked zone, ε_0 is the strain at cracking, $\boldsymbol{f_t}$ is the tensile strength of concrete, $\boldsymbol{\alpha}$ is the softening parameter which can be defined as follows:

$$\alpha=(\boldsymbol{G_f}-\boldsymbol{f_t}\varepsilon_0\boldsymbol{l_c}/2)/\boldsymbol{f_t}\cdot\boldsymbol{l_c}>0 \tag{6}$$

in which, $\boldsymbol{l_c}\approx(\boldsymbol{dv})^{1/3}$, $\boldsymbol{dv}$ is the volume of concrete represented by the sampling point; $\boldsymbol{G_f}=\int_0^\infty \boldsymbol{\sigma dw}$ = the energy needed to separate the two crack surfaces ≈50-200 N/m; $\boldsymbol{w}=\boldsymbol{l_c\varepsilon_c}$=the fictitious crack width. It should be noted that this computation of strain-softening branch of the stress-strain curve is only directly applicable to plain concrete. The classical "tension stiffening" effect due to the presence of reinforcing bars has not been accounted for. The effect of the reinforcement or steel plate can be included by taking a higher fracture energy for reinforced concrete or concrete-filled steel tube than for plain concrete.

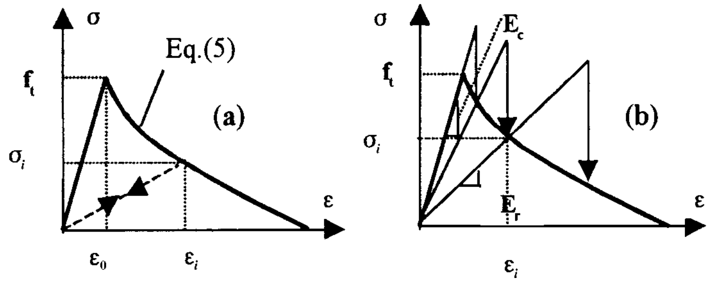

Fig. 3 Tension-stiffening curve

During the loading process a previously opened crack can begin to close and eventually close totally or re-open again. This behavior is allowed in the present model. If the current strain ε is smaller than the strain ε_i recorded as the maximum tensile strain reached across the crack under consideration, the stress normal to the crack is calculated from

$$\sigma=\frac{\sigma_i}{\varepsilon_i}\varepsilon \tag{7}$$

This secant "unloading" path is shown in Fig. 3(a). Re-opening of the crack follows the same path until ε_i is exceeded. Then the stress is interpolated from Eq. (5). Once a crack is completely closed, the concrete is assumed to recover its initial compressive strength normal to the crack.

2.4. The crack [*D*] matrix

Once cracked, the concrete is assumed to become orthotropic with the material axes oriented in the direction of the principal tensile stresses. The [$\boldsymbol{D}$] matrix is constructed with reference to the material axes and it is then transformed into the global system. At cracked sampling points, Poisson's ratio is assumed equal to zero, and the [$\boldsymbol{D}$] matrix thereby becomes a diagonal matrix. The elastic modulus is usually assumed to equal zero in the directions normal to cracked planes, which can sometimes lead to non-positive-definite stiffness matrices and subsequent numerical difficulties. This paper assumes a progressively decreasing stiffness in the considered direction, that is, uses a secant elastic modulus for the [$\boldsymbol{D}$] matrix. The secant modulus, $\boldsymbol{E_r}$, can be evaluated as (see Fig. 3b)

$$\boldsymbol{E_r}=\boldsymbol{\sigma_j}/\boldsymbol{\varepsilon_j}\leq \boldsymbol{E_c} \tag{8}$$

The resulting [$\boldsymbol{D}$] matrix for two-cracked concrete has the form

$$\{\Delta\sigma\}=[\boldsymbol{D}]\{\Delta\varepsilon\}=\text{diag.}[\boldsymbol{E}_{r1}\ \boldsymbol{E}_{r2}\ \boldsymbol{E}_{c}\ \beta_1\boldsymbol{G}\ \beta_2\boldsymbol{G}\ \beta_1\boldsymbol{G}]\{\Delta\varepsilon\} \tag{9}$$

For one-cracked concrete, $\boldsymbol{E}_{r2}=\boldsymbol{E_c}$, $\beta_2=1.0$. As can be seen in Eq. (9) the shear modulus is also modified for cracked concrete, accounting for phenomena such as aggregate interlock, etc.. The shear retention factor is usually given a value of $\beta_1=\beta_2=\beta=0.5$.

3. Material model for steel

In the present work the steel element is assumed to be Von Mises elasto-plastic model with isotropic hardening, and the derivation of whose stiffness matrix can be found elsewhere (Bangash 1998). Unloading is assumed to occur elastically.

4. Finite element model and nonlinear solution techniques

4.1. 3-D element

In the present work, steel and concrete of CFRT column are discretized into 20-node isoparametric element, whose stiffness matrix can be found elsewhere (Bangash 1989). The $3\times3\times3$ Gaussian product rules exactly integrate the stiffness matrix of the 20-node elements (for elements with constant Jacobian and with constant material properties throughout the element). The $2\times2\times2$ reduced integration is used herein to save computation time, because it greatly reduces the number of operations to be performed in the evaluation of the residual forces and tangential stiffness matrices. However, it is well known that under-integrated matrices are rank deficient and can lead to the development of spurious deformation mechanism. By trying and calculating, it is found that the spurious deformation mechanism can be depressed if the aspect ratio of individual 20-node solid element is limited to a maximum of 20. Also reduced integration can alleviate shear-locking behavior resulting from the spurious shear strains.

4.2. Solution of nonlinear equations and convergence criteria

The incremental equilibrium equations in the nonlinear analysis of concrete structure can be expressed as

$$[\boldsymbol{K}]^{i-1}\{\Delta\boldsymbol{U}\}^{i}=\{\Delta\boldsymbol{R}\}^{i}+[\boldsymbol{R}]^{i-1}-\sum_{e}\int_{v}[\boldsymbol{B}]^{T}[\boldsymbol{\sigma}]^{i-1}d\boldsymbol{v}=\{\Delta\boldsymbol{R}\}^{i}+[\boldsymbol{\Psi}]^{i-1} \tag{10}$$

where $[\boldsymbol{K}]^{i-1}$ is stiffness matrix, $\{\Delta\boldsymbol{R}\}$ is the vector of incremental applied loads, and $\{\boldsymbol{\Psi}\}$ is the vector of residual or “unbalanced” forces. The modified Newton-Raphson iterative method is used to solve the nonlinear equation where the tangential stiffness matrix is updated once during an increment. The vector of incremental applied loads $\{\Delta\boldsymbol{R}\}$ and the vector of residual force $\{\boldsymbol{\Psi}\}$ are checked in every iteration and convergence is achieved when

$$\|\{\boldsymbol{\Psi}\}\| \le 0.02\|\{\boldsymbol{\Delta R}\}\| \tag{11a}$$

$$\max|\{\boldsymbol{\Psi}_i\}| \le 0.02\|\{\boldsymbol{\Delta R}\}\| \tag{11b}$$

Eq. (11a) compares the Euclidean norms (square root of the sum of the squares) of the two vectors and represents an average check on equilibrium. The second check Eq. (11b) is to detect any highly localized values in the residual load vector; both checks must be satisfied for reaching convergence.

5. Verification of the model and further application

To verify the above method, comparison of finite element results with the tested results of CFRT short columns made by the authors (Report of Joint Research of Tongji University and Fujita Co. of Japan 1997) and Tomii (1977) is made. Table 1 shows the parameters of specimens and the comparisons of ultimate load capacity. In Table 1 most of the predicted ultimate capacity underestimate the experimental loads by about 2%-16%. This discrepancy may result from (i) during tests, the friction between column ends and loading plates is not considered in the analysis, which leads to lower calculated values than tested ones; and (ii) the material strength of the specimens are scatter somewhat, for example, the tested ultimate capacity of specimen CFRT40-4 is higher than that of CFRT40-5 by 3%. Overall, the finite element method gives reliable prediction and can meet the requirement of engineering accuracy on the safe side.

Due to the limited page number, only the experimental and analytical results of specimen

Table 1 comparison of predicted ultimate load capacity with tested ones

Specimen No.	Section (mm)	f_c (MPa)	E_c (MPa)	Height (mm)	Tested capacity N_U (kN)	Predicted capacity N_U^c (kN)	$\frac{N_U^c}{N_U}$	Steel parameter
CFRT40-3	200×200	24.7	30000		2061	1937	0.94	
CFRT40-4	$\times5$	28.3	27800	600	2530	2115	0.84	
CFRT40-5		32.5	28100		2468	2227	0.90	σ_s =227Mpa
CFRT60-3	300×300	24.7	30000		3621	3569	0.98	σ_b =366Mpa
CFRT60-4	$\times5$	28.3	27800	900	4603	4023	0.87	E_s =214000Mpa
CFRT60-5		32.5	28100		4872	4381	0.90	
I-A*	100×100	32.6			507	481	0.94	σ_s =198Mpa
I-B*	$\times2.29$		30000		508		0.94	σ_b =353Mpa
II-A*	100×100	21.8			521	513	0.98	σ_s =346Mpa
II-B*	$\times2.20$		30000	300	520		0.98	σ_b =419Mpa
III-A*	100×100	21.0			539	551	1.02	σ_s =294Mpa
III-B*	$\times2.99$		30000		538		1.02	σ_b =412Mpa
IV-A*	100×100	20.2			680	689	1.01	σ_s =290Mpa
IV-B*	$\times4.25$		30000		679		1.01	σ_b =400Mpa

*Data comes from Tomii (1977). In analysis, E_c =30000 Mpa, E_s =200000 Mpa.

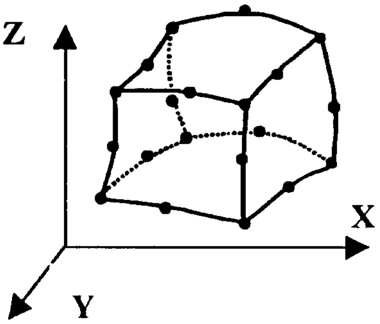

Fig. 4 20-node isoparametric element

CFRT40-5 are given herein for clarification. Considering the symmetry of the specimen, only 1/4 of the specimen is discretized into steel and concrete solid element and the finite element mesh is shown in Fig. 5 with 102 steel elements, 384 concrete elements and 2560 nodes. The fracture energy G_f of concrete is 100 N/m due to the fact that its value has minor effect on the ultimate capacity when it has the values between 50 and 150 N/m.

Fig. 6 gives a comparison of analytical and experimental results, which only consist of the results before the steel is locally buckled since the effect of local buckling is not considered in the present model. Fig. 7 shows the state of steel and concrete elements at the central height of the column during loading. Fig. 7a shows the state corresponding to the load of $1/2N_u^c$(N_u^c is the calculated ultimate load capacity). At this load level, all steel elements are elastic and only the concrete elements crack in the corner zone of the section. These corner cracks are stable in the later loading

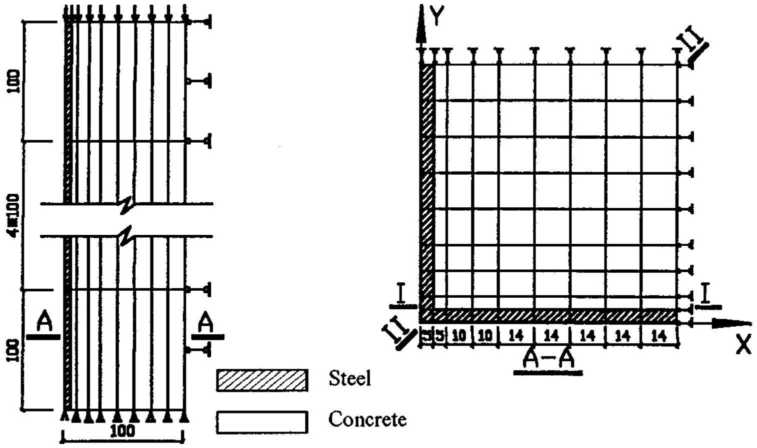

Fig. 5 Finite element mesh of specimen CFRT 40-5

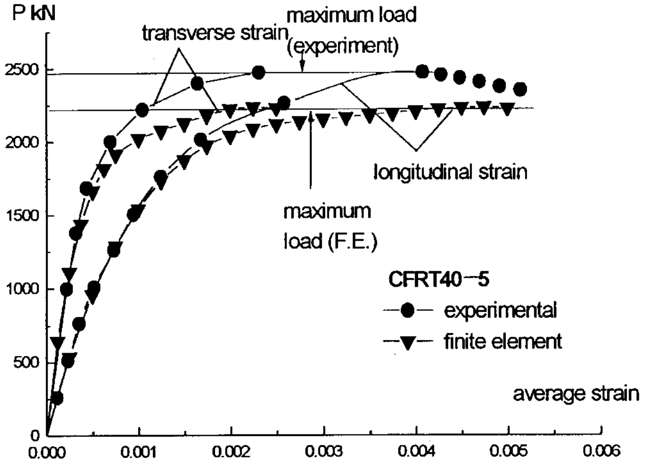

Fig. 6 Load-deformation curves

stage due to confinement provided by steel tube. It must be noted that one should interpret the terminology "crack" judiciously because a physical crack does not actually develop at the element integration point, instead, the material has failed in one principal stress direction. Fig. 7b shows the states corresponding to the load level of N_u^c. At this load level, all the steel elements yield and cracked concrete elements develop along the side zone. A small part of concrete in the center of the section is uncracked and most of concrete elements in the diagonal zone soften with increasing compressive strain. These results indicate that confinement effect of CFRT section is concentrated on the corner zone, and those corner concrete elements carry most of the longitudinal and transverse stresses. Thus, it can be concluded that the load capacity of inner concrete of CFRT column depends on the two diagonal zones.

Fig. 8 and Fig. 9 show the transverse stress distribution of concrete elements at I-I and II-II sections (see Fig. 5) respectively, where compressive stress is positive and tensile stress is negative. General trend of stress distribution can be found from the two figures as follows: (i) along the side

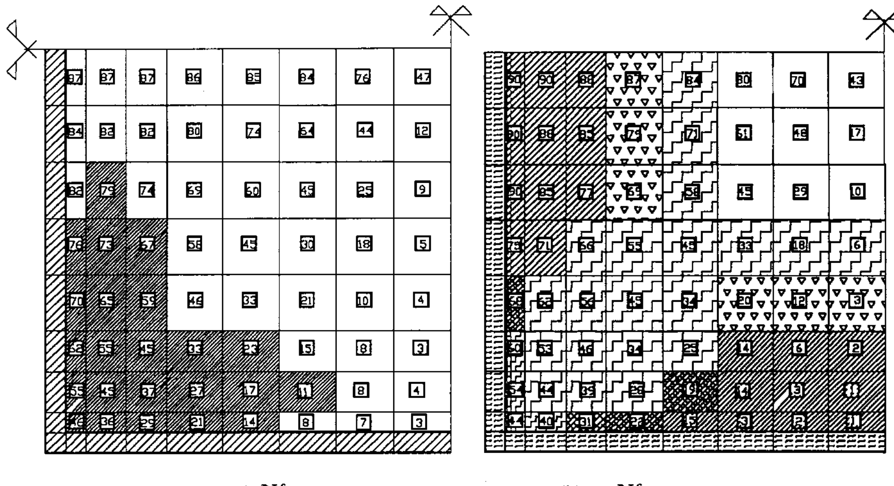

(a) $P=1/2\,N_u^c$ (b) $P=N_u^c$

Fig. 7 Failure state of concrete and steel elements

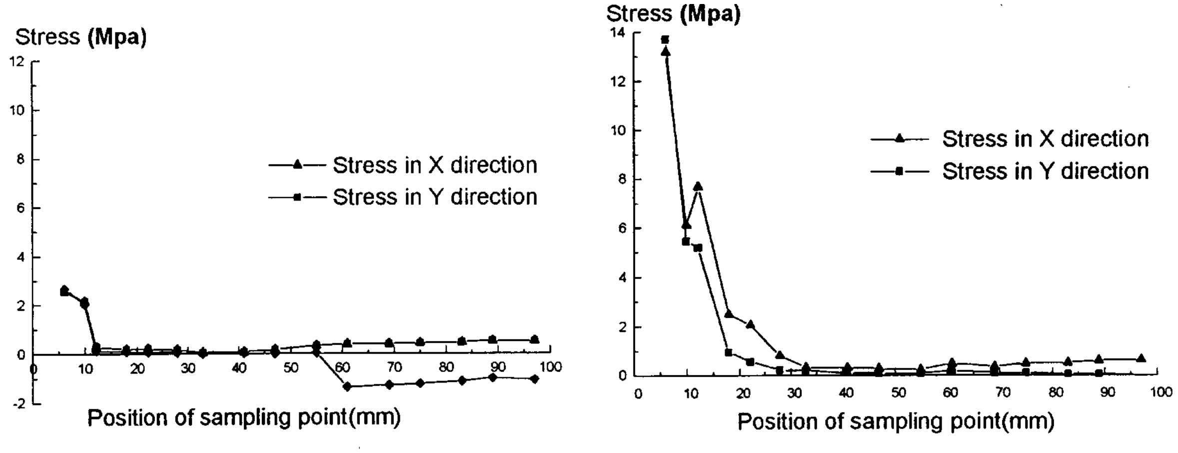

(a) $P=1/2\,N_u^c$ (b) $P=N_u^c$

Fig. 8 Transverse stress distribution of concrete elements in I-I section

direction (I-I section), $\sigma_x \neq \sigma_y$, but difference between stress in two directions is small for most part of I-I section, also confining stress decreases rapidly from the corner zone to the central part; (ii) along the diagonal elements (II-II section) $\sigma_x \approx \sigma_y$, and confining stress in the corner zone is maximum and decreases rapidly along the central part direction; (iii) at load level of $1/2N_u^c$, the stress σ_y of the central elements in I-I section is tensile stress, which can be explained as follows: at

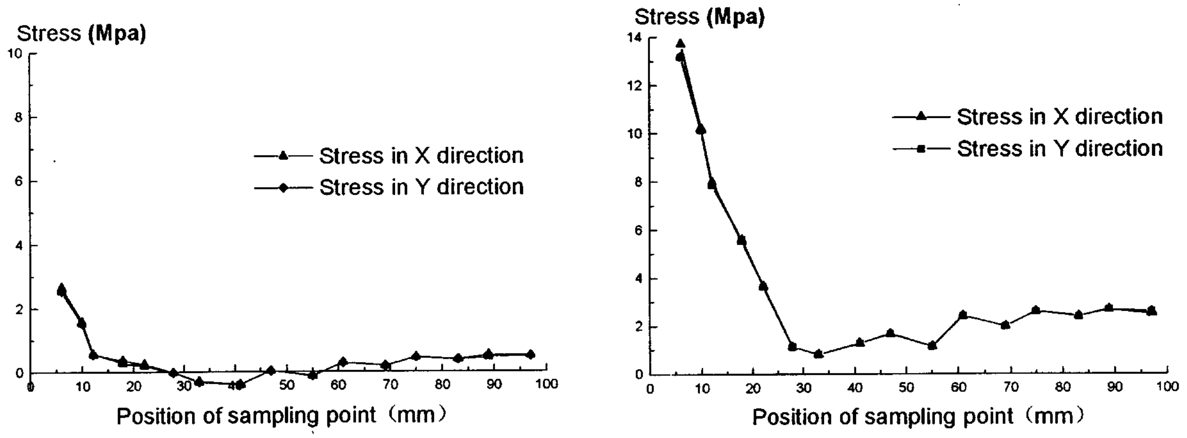

(a) P=1/2 N_u^c (b) P= N_u^c

Fig. 9 Transverse stress distribution of concrete elements in II-II section

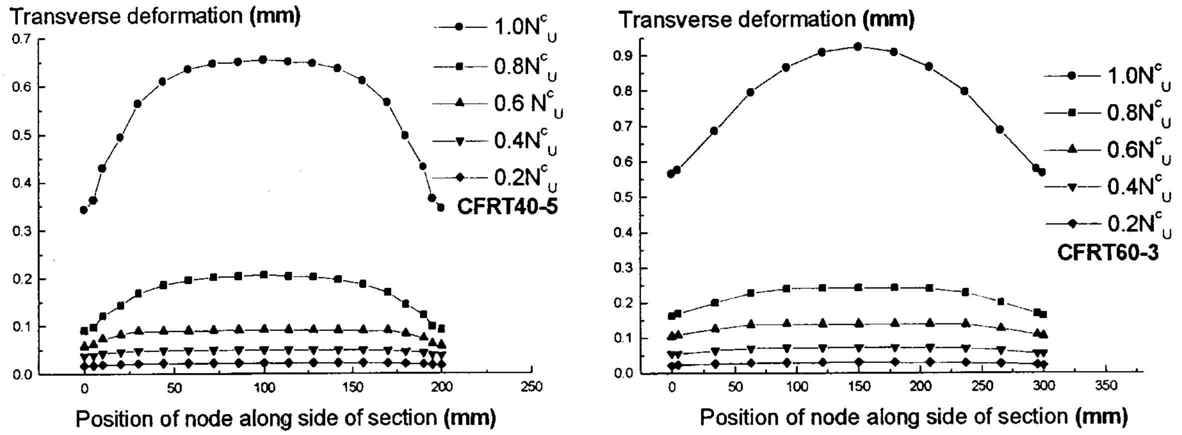

(a) Specimen CFRT40-5 (b) Specimen CFRT60-3

Fig. 10 Predicted transverse deformation of CFRT column during loading

the earlier load stage, the Poisson's ratio of concrete is smaller than that of steel, and the separation trend between two materials results in tensile stress, which should not exceed the bond strength, but may be overestimated in this paper due to the assumption of perfect bond between concrete and steel tube wall. Fig. 10 shows the transverse deformation of CFRT section during loading. As seen from the figure, transverse deformation of central part of the section increases and exceeds that of corner part as the loading increases, which reproduces the phenomena observed during experiment. From the above analysis, it can be concluded that confining effect of CFRT section is mainly concentrated on the corner zones, which is different from concrete-filled steel circular tube and from concrete section confined by rectangular stirrups.

6. Conclusions

The proposed finite element model for the nonlinear static analysis of three-dimensional CFRT columns can evaluate the capacity and deformation behavior of CFRT columns well. It needs only a few inputted data and is stable during analysis. Therefore it provides an effective tool for studying the structural behavior and inherent mechanism of CFRT composite structures.

Finite element analysis results indicate that the capacity of inner concrete of CFRT column mainly depends on the two diagonal zones. At ultimate state, the side concrete along the of the section cracks seriously and the corner concrete softens with the increase of compressive strains until failure. Distributions of transverse stresses also show that confining effect of CFRT section is mainly concentrated on the corner zones, which is different from concrete-filled circular tube and from concrete section confined by rectangular stirrups.

References

Bangash, M.Y.H. (1989), *Concrete and Concrete Structures: Numerical Modeling and Applications*, Elsevier Applied Science, London and New York, 74-80.

Jiang, Jianjing (1993), *Nonlinear F.E.M. Analysis of R.C. Structures*, Xi An, Shaanxi Science and Technology Publish Association, 7-11(in Chinese).

Neogi, P.K. and Sen, H.K. (1969), “Concrete-filled tubular steel columns under eccentric loading”, *The Struct. Engr.*, **47**(5), 187-195.

Report of Joint Research of Tongji University and Fujita Co. of Japan (1997), “Experimental study of CFRT short column under concentric loading”, 23.

Shakir-Khalil, H. and Zeghiche, Z. (1989), “Experimental behavior of concrete-filled rolled rectangular hollow section columns”, *The Struct. Engr.*, **67**, 345-353.

Tomii, M. (1977), “Inelastic behavior of concrete filled steel tube beam-columns”, *Colloquium on Stability of Structures under Static and Dynamic Loads*, Washington, USA.

Tomii, M. and Sakino, K. (1979), “Elasto-plastic behavior of concrete filled square steel tubular beam-columns”, *Trans., Arch. Inst. Japan*, **275**, 55-63.

Yu Yong and Lu Xilin (1998), “A 3D constitutive relationship of confined concrete”, *Journal of Tongji University*, **26**(6), 622-626 (in Chinese).